The 3rd International Conference on Water Resources and Arid Environments (2008)
and the 1st Arab Water Forum

Estimation of Evapotranspiration Using Fused Remote Sensing Image Data and M-Sebal Model for Improving Water Management in Arid Mountainous Area

Ayoub Almhab and Ibrahim Busu
Department of Remote Sensing, Faculty of Geoinformation
science & engineering, Universiti Teknologi, Malaysia

Abstract

Remote sensing has been proven to be very useful in the investigation of vegetation and hydrological monitoring, especially when looking at vast areas. In this paper, the complementarily between two optical remote sensing data (Landsat TM and NOAA- AVHRR) and a Digital Elevation Model (DEM) is used to estimate hydrological parameters according based on derived surface reflectance these parameters used in the Modified - Soil Energy Balance Algorithm for Land (M-SEBAL) model, using data from Landsat TM and NOAA-AVHRR sensors, has been used to estimate net radiation, soil heat flux, sensible heat flux and ET for Sana'a Basin in Yemen. The area is known for arid and semi-arid weather conditions with undulating topography. Image data from AVHRR on-board NOAA satellites with a large areal coverage, good temporal and spectral resolution are found to be very useful in generating some parameters required for the above process. However, the data lack pure spatial resolution. On the other hand, image data from Thematic Mapper on-board LANDSAT satellite, with a high spatial and spectral resolution should be able to provide values for the parameters involved, but the areal coverage is significantly reduced. The study has been carried out, using both image data through a data fusion technique in order to harvest advantages and goodness of these two image data, a general framework is proposed to generate evapotranspiration maps for arid and semi-arid regions. This is achieved by means of multi-temporal, multi-resolution remote sensing data. considering topographic effects, an attempt has also been made to incorporate DEM information for estimating the net radiation of the areas involved. An application for computing daily evapotranspiration (ET) map over Sana'a Basin, a central mountainous region in Yemen is presented. As a result, a daily ET map generated from metrological observation was compared with estimated ET data simulated from remote sensing data. In conclusion, data from both remote sensing give reasonable values with result from TM being better when compared with those of AVHRR.

This is attributed to the differences in spatial resolution, in which TM data is higher than AVHRR.

Keywords: Evapotranspiration; TM; AVHRR; SEBAL; Yemen.

Introduction

Evapotranspiration (ET), as part of the hydrological cycle, is affected by many processes at the interface between soil, vegetation and earth's atmosphere. A number of models for ET estimation have been presented: empirical, semi-empirical models and physical models. These models have increased the precision of ET estimation (Brutsert, 1979). There are many methods available to estimate reference ET using meteorological data: FAO-24 (Doorenbos, and Pruitt, 1977), FAO-56 (Allen, et. al 1998). Reference ET can be defined as the ET rate of a reference crop expressed in inches or millimeters. Most of these methods are based on point data, which do not provide a good estimation of ET for large areas (Tuya, et al, 2005). The problem of actual ET estimation over a large area can be solved using remote sensing methods that provide ET on pixel-by-pixel basis. Many researchers (Vidal and Perrier, 1989, Granger, 1989, Bastiaanssen, 1995, 2000, Bastiaanssen, et al.,1998, 2005, Tasumi,et al, 2000, Almhab et al,2007a,b,c and Almhab & Busu. 2008) have already developed various methodologies by combining of satellite and ground data for large areas since the 1990s. This study focuses on the estimation of actual ET using M-SEBAL. ET in general consists of 99% of the crop water requirements. Thus, the agriculture monitoring is necessary for efficient food produce and security management at state level. Typically, monitoring requirement from the point of view of an agricultural or irrigation manager would be to monitor each field at regular interval such as every 7 days is seems reasonable. ET is encompassing the water in crop, and it is therefore a crucial indicator of crop productivity. It can be estimated from remote sensing data. However, the availability of high spatial resolution data from satellite remote sensing is very limited as supposed to the low spatial resolution data, which available daily (even 7 days composites image data are ready available on the internet). in order to overuse this problem, marching or fusing the two satellite image data of high and low spatial resolution to enhance ET (chemin et al , 2004). One area of work which is related to data fusion is the fusion of data for improving the spatial resolution of multitemporal images, a technique which is directed towards fusing comparatively high spatial resolution and low temporal resolution satellite images with other images, high temporal and low spatial resolution, thus achieving better spatial and temporal resolution with the fusion of the images. While spectral/spatial fusion is relatively common, the spatial/temporal fusion is still in its infancy. There are several reasons for that; the first and foremost is that the observed Earth surface is variable with time. Secondly, and as a direct corollary, the nature of the information derived from the satellite data is never constant, else specific cases of Albedo values on typically

invariant features (Chemin, 2002). When considering quantitative information, like the evapotranspiration, the first concern is to keep the volumes of water constant through the scales, in other words, the sum of water volume evapotranspired from small size pixels should be equal to the water volume in the large pixel of another satellite that encompasses the smaller pixels. This paper present investigation aims at:

-Describing the implementation issues of modified SEBAL (M-SEBAL) whereby the ET data from remote sensing images could be used to generate ET data, with different processing levels, NOAA-AVHRR and LANDSAT-5 TM data, to compute spatially distributed ET by remote sensing over an arid and semi-arid region with mountainous terrain areas in Yemen.
- Studying the feasibility of fusion ET result using M-SEBAL from NOAA-AVHRR and LANDSAT-5 TM data and compare between the two.
-Comparing M-SEBAL ET with soil water balance (lysimeter) ET.

Material and Method

1 Research Area

The Sana'a Basin is located in the western highlands of Yemen opposite the Red Sea and the Gulf of Aden (figure 1). It is mostly an intermountain plain surrounded by highlands from the west, south and east. On a regional scale, the Basin extends across the central part of the Sana'a Governorate and covers about 24% (3250 km2) of its total area (13,550km2).

There is a significant variation in altitude both east-west and north-south. The highest point in the Basin is in the southwest end (Jabal An Nabi Shu'ayb) and has an elevation of almost 3700 m above see level (m.a.s.L) The lowest which is (about 1900 m.a.s.l.) is in the northern extremity where the Wadi Al Kharid exits and this is the main basin. The predominant climate is arid, although semi-arid conditions prevail in localized areas, particularly along the western highlands.

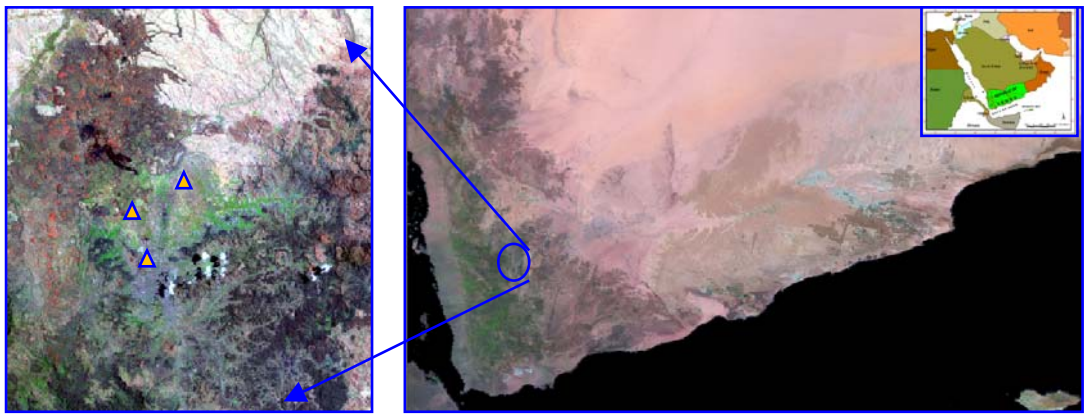

Fig. 1. The central Yemen mountains as seen on a True -color Landsat image acquired on june 1st (1998).
△ location of the climatic station in Sana'a basin.

2. Dataset

Satellite images from tow different satellite images one NOAA-AVHRR and one LANDSAT5-TM , were evaluated for Land Surface Heat Fluxes distribution in Sana'a basin central Yemen mountains. The overpass time of these images was 10.30of LANDSAT5-TM and 14.00 of NOAA-AVHRR local time. Both images had favorable weather conditions with little clouds in the study area. Data from the field measurement area were available to assist the calculation of the Land Surface Heat Fluxes in the locations of the study area (Lat: 15.3 N, long: 43.15 E).

Table 1. NOAA-AVHRR and LANDSAT TM image acquisition dates for the integration

N0.	NOAA-AVHHR	Landsat
1	March 31	Mar 26
2	June 10	Jun 1
3	Oct. 23	
3	Dece. 20	Dece. 12

3. Model

A Modified SEBAL model was developed by introducing some changes into the existing SEBAL model. Notably these were the inclusion of terrain, mountains and deserts effect in to calculations of surface radiation. The modified SEBAL model was calculated using model builder in ERDAS IMAGINE 8.5 image processing package. All model parameters were programmed into the model builder and values are computed automatically based on the input data. The general flowchart for the modified SEBAL model is shown in Figure 2.

The method uses the energy budget equation to calculate each pixel $\lambda(ET_{ins})$ (instant latent heat loss) at the time of the satellite over flight.

$$\lambda\left(ET_{ins}\right) = R_n - G - H \qquad \text{Eq. 1}$$

where: $\lambda(ET_{ins})$ is the instant latent heat loss (w/m^2) , which is calculated as a residual of the energy budget, λ is the latent heat (i.e. the heat needed to evaporate unit mass of water), ET_{ins} is the rate of evapotranspiration at the time of the satellite overflight, R_n is net solar raids (w/m^2), G is soil heat flux into the soil (w/m^2), H is the sensible heat flux into the air (w/m^2).

4 Theory

4.1 Net Radiation (R_n) : The radiation balance at the Earth's surface is composed of four spectral radiant fluxes, the incoming short wave (0.14 to 4 μm) radiation that arrives from the sun ($R_{s\downarrow}$), the amount of this energy that is reflected from the surface ($R_{s\uparrow}$), the incoming long wave (> 4 μm) radiation from the atmosphere ($R_{L\downarrow}$), and the amount of long wave radiation emitted from the surface ($R_{L\uparrow}$). Thus the net radiation is:

$$R_n = R_{s\downarrow} - R_{s\uparrow} + R_{L\downarrow} - R_{L\uparrow} \qquad \text{Eq. 2}$$

The instantaneous net amount of radiation received by a surface can be written in the form:

$$R_n = (1-\alpha)R_{s\downarrow} + \varepsilon_a \sigma T_a^4 - \varepsilon_s \sigma T_s^4 \qquad \text{Eq. 3}$$

where R_s is the incoming short-wave solar radiation, α is the surface short-wave albedo, σ is the Stefan–Boltzmann constant (5.67 x 10^{-8} W m^{-2} K^{-4}), T_a is the air temperature measured at the wet pixel (K), T_s derived from a remotely sensed radiometric surface temperature (K), ε_a is the air emissivity taking as [Bastiaanssen, 1995]:

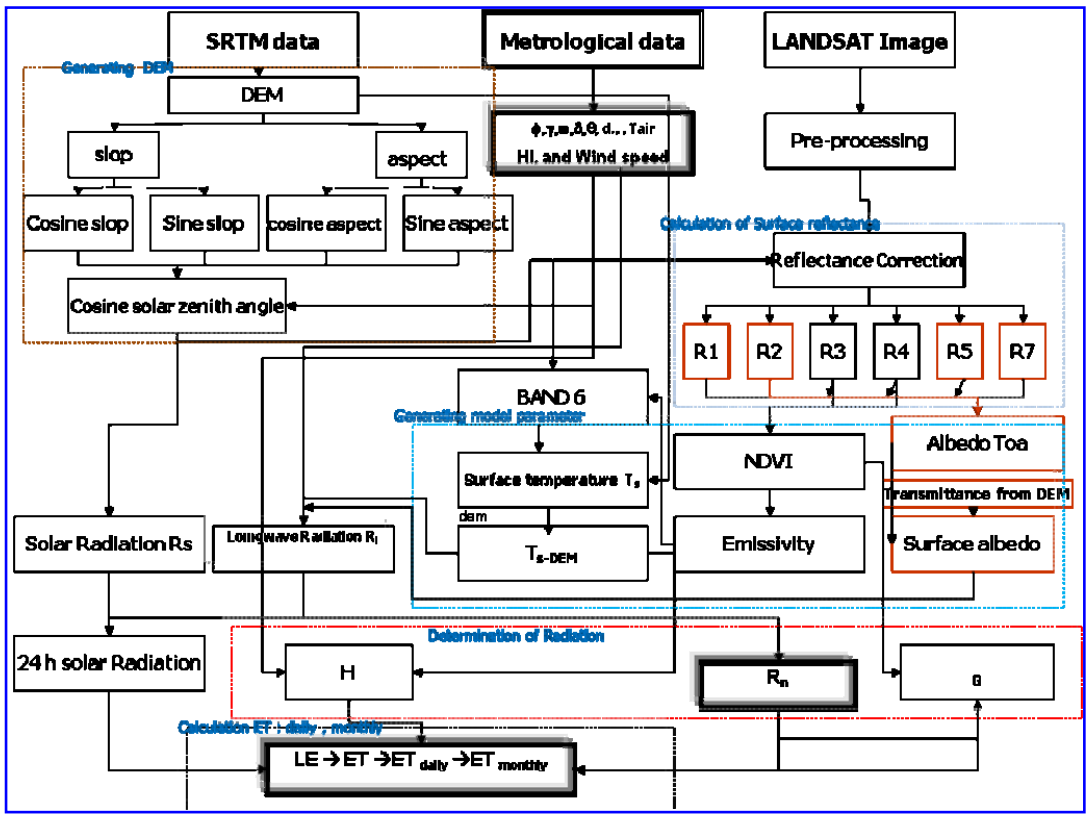

Ri is the Reflectance correction band I,

Figure 2 The general flowchart of correlations between modified SEBAL model parameter

$$\varepsilon_a = 1.08(-\ln \tau_{sw})^{0.265} \qquad \text{Eq. 4}$$

where τ_{sw} is two way atmospheric transmissivity [τ_{sw} = 0.75+2x10^{-5} z],z is elevation meter. where ε_s= surface emissivity which is calculated from normalized vegetation index (NDVI) using the logarithmic relation of Van de Griend and Owe (1993) as:

$$\varepsilon_s = 1.0094 + 0.047 * \ln(NDVI) \qquad \text{Eq. 5}$$

The weighting factors for each band are the proportions of solar radiation incident at the earth surface in each segment. This approach was adopted here to derive α from narrow bands. α is calculated by the equation in Tasume et al. (2000)for LANDSAT surface reflectance data.

$$\rho^{TOA} = 0.293\rho 1^{TOA} + 0.274\ \rho 2^{TOA} + 0.233\ \rho 3^{TOA} + 0.157\ \rho 4^{TOA} + 0.033\ \rho 5^{TOA} + 0.011\rho 7^{TOA} \quad \text{Eq. 6a}$$

ρi is the reflectance for LANDSAT data band i. We adopted the equation of Chemin et al. (2000) for NOAA-AVHRR surface reflectance data.

$$\rho^{TOA} = 0.035 + 0.0545\rho 1^{TOA} + 0.32\ \rho 2^{TOA} \quad \text{Eq. 6b}$$

ρi is the reflectance for NOAA-AVHRR data band i.

The incoming short wave radiation *($R_s\downarrow$)* was computed in this study, by equation (7) as follows (Fu 1998, Tasuni et al. 200) in which the diffuse radiation was neglected:

$$R_s\downarrow = \frac{G_{SC}}{d^2_r}\cos\theta \times \tau \quad \text{Eq. 7}$$

where G_{sc} is the solar constant(1367 w/m^2), d_r is inverse squared relative distance earth-sun (dimensionless) calculated by $dr=1+0.033\cos\{[2\pi(DOY)]/365\}$, $\cos\theta$ is cosine of the solar zenith angle calculated by $\cos\theta=\cos(\pi/2-\phi)$ where ϕ is sun elevation angle in radians (in the flat area) in the slop and mountain terrain areas (like our case study) solar incident angle changes with surface slope and aspect. Therefore the equation suggested by Duffie and Bekman,(1991) is applied.

$$\cos\theta = \sin(\delta)\sin(\phi)\cos(s) - \sin(\delta)\cos(\phi)\sin(s)\cos(\gamma) + \cos(\delta)\cos(\phi)\cos(s)\cos(\omega) + \cos(\delta)\sin(\phi)\sin(s)\cos(\gamma)\cos(\omega) \quad \text{Eq. 8}$$

where: δ is solar declination(rad); ϕ is geographic latitude of the pixel (rad); s is ground slope (rad); γ is the surface aspect angle (rad); ω is the hour angle of the sun(rad).

4.2 Soil Heat Flux (*G*):

Soil heat flux is usually measured with sensors buried just beneath the soil surface. A remote measurement of G is not possible but several studies have shown that the day time ratio of G/R_n is related to among other factors, such as the normalized difference vegetation index(NDVI). In this study equation (9) is adapted with the figure 3 showing the regression equation.

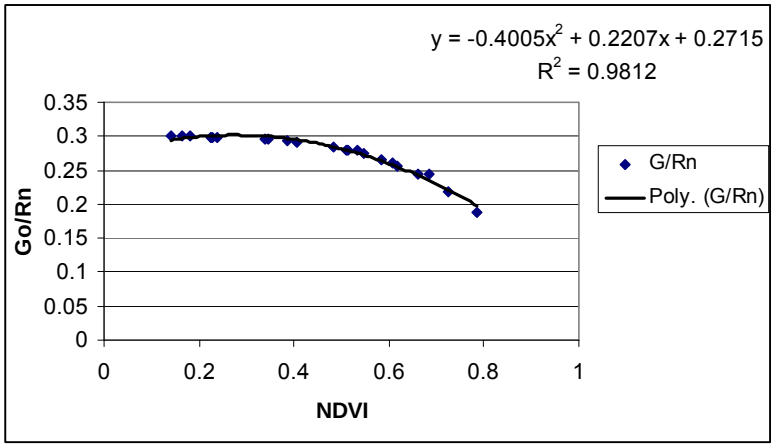

Figure 3. The regression equation for G/R_n.

G as an empirical fraction of the net radiation using surface temperature, surface albedo (α) and NDVI and was adopted here to compute G as:

$$G = R_n\left(-0.4005NDVI^2 + 0.2207NDVI + 0.2715\right) \quad \text{Eq. 9}$$

where T_s is the surface temperature, NDVI is the normalized difference vegetation index. □ is calculated as the following:

$$NDVI = (R_4 - R_3) / (R_4 + R_3) \quad \text{Eq. 10}$$

where R_4 and R_3 are the reflectance data of bands 4 and 3 in LANDSAT and bands 2 and 1 in NOAA-AVHRR respectively.

4.3 Sensible Heat Flux (*H*):

For the sensible heat flux calculation, two pixels are chosen in the satellite data. One pixel is a wet pixel that is a well-irrigated crop surface with full cover and the surface temperature (T_s) close to air temperature (T_a) The second pixel is a dry bare agricultural field where λE is assumed to be 0. The two pixels tie the calculations for all other pixels between these two points. At the dry pixel, assume λE =0, then according to equation (1) and the definition of specific heat capacity

$$H = R_n - G \quad \text{Eq. 11}$$

$$H = \frac{\rho c_p dT}{r_{ah}} \quad \text{Eq. 12}$$

where ρ is the air density (mol m^{-3}), c_p is the specific heat of air (29.3 J mol^{-1} $^oC^{-1}$), d*T* is the near surface temperature difference (K), r_{ah} is the aerodynamic resistance to heat transport m/s, where

$$r_{ah} = \frac{\ln\left(\frac{z_2}{z_1}\right)}{u^* k} \qquad \text{Eq. 13}$$

z_1 is a height just above the zero displacement distance height of plant canopy set to 0.1 m for each pixel, and z_2 is the reference height just above the plant canopy set to 2 m for each pixel, u* is the friction velocity (m/s), and k is the von Karman constant (0.4).

$$u^* = \frac{u(z)k}{\ln(\frac{z-d}{z_m})} \qquad \text{Eq.14}$$

where $u(z)$ is the wind speed at height of z, d is the zero displacement height (m, d=0.65h), h is the plant height (m), and z_m is the roughness length (m, z_m=0.1h)[Campbell and Norman 1998]. According to equations 13-14 and the input data, dT_{dry}, dT at the dry spot can be calculated. At the wet spot, assume H=0 and dT_{wet} =0 (dT at the wet spot). Then according to the surface temperature at the dry and wet spots (T_{sdry} and T_{swet}), we can get one linear equation for each pixel (wing et al, 2006),

$$dT = \left(\frac{dT_{dry} - dT_{wet}}{T_{s\,dry} - T_{s\,wet}}\right) \times T_s - \left(\frac{dT_{dry} - dT_{wet}}{T_{s\,dry} - T_{s\,wet}}\right) \times T_{s\,wet} \qquad \text{Eq. 15}$$

Then, according to the equation, the H each pixel can be calculated according to equations 11-14. We assumed at 200 m the wind speed is the same for each pixel and the wind speed at 200 m is calculated for the weather station first, and then u* can be solved for each pixel (equation 14). The parameter d in equation 14 is set to 0 which is negligible when z =200 m. The z_m for each pixel is calculated by a regression equation according to the pixel value. The equation is obtained by three pairs of known values of z_m and $NDVI$. For example if we know that Anguses tree (maturity growing) has z_m =*1.1* m and *NDVI=0.464*, for alfalfa z_m =0.03 m and NDVI=0.248, and bare agricultural field z_m =0.00 m and NDVI=0.113, then we can obtain a regression equation for z_m (Figure 4).

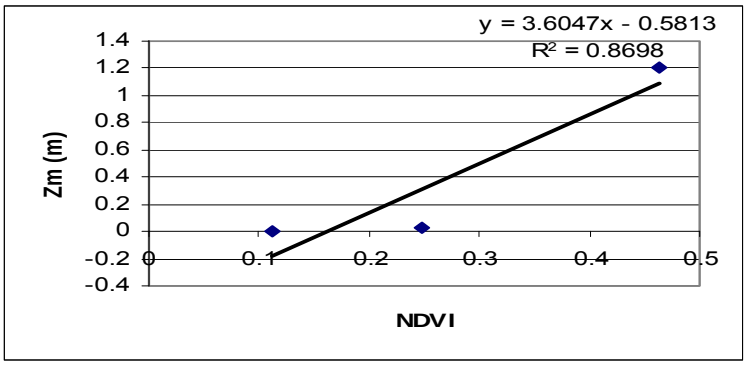

Figure 4. One example of a regression equation for z_m from NDVI.

Due to the fact that atmospheric stability may have effects on H, the atmospheric correction is conducted (16). First the u* and wind speed at 200 m at the local weather station are calculated. Then the z_m, u^* and dT for each pixel are computed. Then the r_{ah} and H without the atmospheric correction are obtained.

For atmospheric correction, the stability parameter, the Obukhove length, L (m) is calculated. Then using the stability parameter, u^*, r_{ah} and H are corrected. Then an iteration is conducted for L, u^*, r_{ah} and H calculation until H does not change more than 10%. The correction equation is as follows (Campbell and Norman 1998; Stull 2001).

$$L = -\frac{u^{*3} T_s}{kgH} \qquad \text{Eq. 16}$$

When L<0, H is positive and heat is transferred from the ground surface to the air, under unstable condition; when L>0, H is negative and heat is transferred from air to ground surface, under stable condition; when L=0, no heat flux occurs, and is under neutral condition, because the satellite over flight occurred at local noon time, the atmosphere should have been unstable. Thus, when a stable condition occurred, we forced L=0 (neutral). After H is corrected by the atmospheric effects, $\lambda(ET_{ins})$ for each pixel is calculated using equation 1.

4.4 Regional ET model:

The actual 24 hour ET can be estimated from the instantaneous evaporative fraction EF, and the daily averaged net radiation, $R_{n,24}$ (Tasumi, et al, 2000):

$$ET_{24} = EF\{R_{n,24}[106(2.501 - 0.002361T_s)]\} \qquad \text{Eq. 17}$$

where ET_{24} is the actual 24-hour evaporation (mm/day), $R_{n,24}$ is the 24-h net radiation (W/m^2), T_s the surface temperature (°C). The EF is the instantaneous evaporative fraction calculated as:

$$EF = \lambda ET / (R_n - G) \quad \text{Eq. 18}$$

where R_n is the instantaneous net radiation and G is the instantaneous soil heat flux.

Finally, the instantaneous latent heat of evapotranspiration (λ ET) may be computed as the residual of the surface energy balance equation (Eq. 1). However, in order to facilitate comparison with the sensible heat flux, is use made of the instantaneous evaporative fraction *EF*, defined as follows :

$$EF = (R_n - G) - H/(R_n - G) \quad \text{Eq. 19}$$

Assuming that the evaporative fraction (*EF*) is constant over the day the daily average sensible heat (H_{24}) can be derived from *EF* and the daily average net radiation (R_{n24}) as follows :

$$H_{24} = (1 - EF) R_{n,24} \quad ((W/m^2)) \quad \text{Eq. 20}$$

The improved daily net radiation parameterization scheme and daily actual evapotranspiration.

The daily net radiation can be expressed as:

$$R_{n24} = (1-\alpha) R_{s24} + R_{L24} \quad ((W/m2)) \quad \text{Eq. 21}$$

where R_{s24} is the daily solar radiation and R_{L24} is the daily net long wave radiation (wm^{-2}).

As the mountain and terrain of our study area is complex with undulations, the impact topography, the impact of slope and azimuth of surface on available radiation shod be considered pixel by pixel in the calculated instantaneous and daily net radiation, the shaded areas (pixels) were excluded from imageries with the model maker in ERDAS imagine software brakeage. Through importing parameters of solar azimuth and solar elevation at the satellite overpass time. The daily net radiation is estimated by an integral of equation (7) transmittance for one-way transmittance τ with ($c+dn/N$):

$$R_{s24} = (c + d\frac{n}{N}) * \int_{-\pi}^{+\pi} \left[\frac{G_{sc}}{d_r^{\,2}} \sin\delta.a + \cos\delta.\cos\omega.b + \cos\delta \sin s.\sin\gamma.\sin\omega \right] d\omega \quad \text{Eq. 22}$$

$$R_{s24} = (c + d\frac{n}{N}) * \int_{\omega 1}^{\omega 2} \left[\frac{G_{sc}}{d_r^{\,2}} \sin\delta.a + \cos\delta.\cos\omega.b + \cos\delta \sin s.\sin\gamma.\sin\omega \right] d\omega \quad \text{Eq. 23}$$

$$R_{a24} = (c + d\frac{n}{N}).\frac{G_{sc}}{2\pi d_r^{\,2}} \left[a.\sin\delta.(\omega_2 - \omega_1) + b.\cos\delta(\sin\omega_2 - \sin\omega_1) - \sin s.\sin\gamma\cos\delta(\cos\omega_2 - \cos\omega_1) \right] \quad \text{Eq. 24}$$

$$a = \sin\phi\cos s - \cos\phi\sin s.\cos\gamma$$
$$b = \cos\phi\cos s + \sin\phi\sin s.\cos\gamma$$

$$N = \frac{12(\omega_2 - \omega_1)}{\pi} \qquad \text{Eq. 25}$$

where: c and d are coefficients of the solar radiation depending on the latitude climate and other factors of study area, respectively; $c+d$ is the fraction of exterritorial radiation reaching the earth on clear sky days. n is the actual sunshine duration, N the potential sunshine duration, ω_1 and ω_2 are the sunrise and sunset angle, respectively. The difficulty in retrieval of the daily solar radiation focuses on calculation of the sunrise and sunset angle for the tilted surfaces.

The sunrise and sunset angles for horizontal surfaces are given by Fu (1983) and Tasumi et al. (2000)

$$\omega_H = \cos^{-1}\left(-\tan\phi.\tan\delta\right) \qquad \text{Eq. 26}$$

The sunrise and sunset angle for tilted surfaces can be obtained by simple mathematical manipulation from equation (8) by setting cosθ=0, leading to

$$\omega = \cos^{-1}\left(\frac{-a.b.\tan\delta \pm \sin\gamma.\sin s\sqrt{1-a^2\left(1+\tan^2\delta\right)}}{1-a^2}\right) \qquad \text{Eq. 27}$$

The positive or negative sign of equation (above) in the numerator are determined by equation:

$$\omega = \sin^{-1}\left(\frac{-a.\sin\gamma.\sin s.\tan\delta \pm b\sqrt{1-a^2\left(1+\tan^2\delta\right)}}{1-a^2}\right) \qquad \text{Eq. 28}$$

Let ω_{s1} and ω_{s2} be the roots of ω, respectively, and $\omega_{s1} > \omega_{s2}$. Note the surface receives the solar radiation only if *cos* θ in equation (8) is greater than 0. several relationships are given below to determine the sunrise and sunset angles (ω_1 , ω_2),

- if $\omega_{s1} \le \omega \le \omega_{s2}$ and cosθ ≥0, then $\omega_{s1} \ge \omega_{s2}$, $\omega_{s2} \le \omega_{s1}$;
- if $\omega \le \omega_{s1}$, $\omega s1 > \omega_{s2}$ and cos>=0 then $\omega_1 \le \omega_{s1}$,$\omega_2 \ge \omega_{s2}$.

Meanwhile, the sunrise and sunset angles for tilted surfaces must also satisty the condition that sunrise is no earlier and sunset is no later than those for horizontal surfaces. Namely $\omega_1 \ge -|\omega_H|$, $\omega_2 \ge \omega_{s2} \le |\omega_H|$.

Daily net long wave radiation:

$$R_{L24} = \varepsilon_a \sigma T_a^4 - \varepsilon_s s T_s^4 \qquad \text{Eq. 29}$$

where ε_a is the daily average atmospheric emissivity (Campbell and Norman, 1998) and T_a is the daily mean atmospheric temperature (k). due to the surface temperature obtain at 10h30, it could represent the daily average surface temperature for estimation of the surface daily long wave radiation (granger, 2000).

5 Fusion Model

The spatial resolution enhancement using M-SEBAL model was applied to satellite images from both the NOAA-AVHRR and Landsat satellite images. NOAA-AVHRR images are characterized by a relatively high temporal resolution (once a day), but a low spatial resolution of approximately 1 km. Landsat images have a high spatial resolution of 30 meter, but a low temporal resolution of 16 days. An analysis of the growing season solely based on Landsat images is practically impossible as the chance of almost all acquisitions during the season being cloud-free is very low in most crops areas. On the other hand, an analysis using only NOAA-AVHRR images would not give sufficient spatial detail. Therefore, the advantages of both sensors are combined in this methodological framework where high and low resolution products are integrated to calculate total seasonal evapotranspiration.

$$ET_{fusion} = ET_{NOAA} x \ ET_{TM}/ET_{TM\text{-}mean} \qquad \text{Eq. 30}$$

$$ET_{fusion\text{-}SEASON} = \sum_{i=1}^{i=3} (ET_{NOAA,i} x \ ET_{TM,j}/ET_{TM\text{-}mean}) \qquad \text{Eq. 31}$$

where i is the NOAA period and j is the corresponding Landsat image. The same method to calculate ET_{seas} is applied to calculate seasonal Evapotranspiration from NOAA-AVHRR and Landsat maps ($m^3 ha^{-1}$) figure 5 showing the general flowchart of the fusion model.

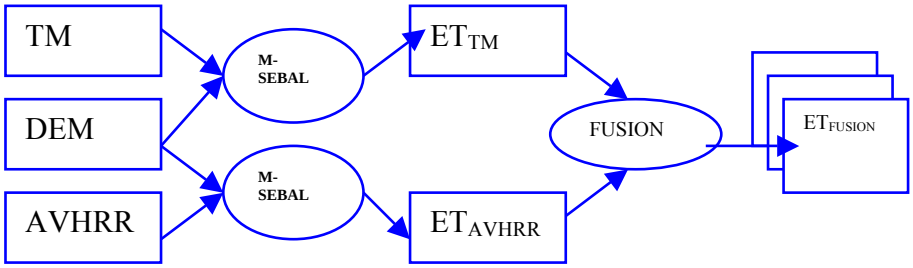

Figure. 5. Scheme for generating daily high resolution maps: mapping individual temporal values on the classification image.

6 Comparison and error analysis of ET.

The measured and simulated is compared. The Relative Error (RE) is calculated as:

$$\mathrm{Re}\,lativeError = \frac{|\,simulation - observation\,|}{observation} \qquad \text{Eq. 32}$$

The Absolute Error (AE) is calculated as (mm/day):

$$AbsoluteError = |\,simulation - observation\,| \qquad \text{Eq. 33}$$

The average of the relative error and the absolute error was also calculated, respectively.

To see if a day was water-stressed in alfalfa field, the non-stressed (alfalfa , mm/day) calculated by FAO Penman-Monteith equation was compared with the corresponding observation. That was obtained from Yemen NWRA Climate Center. The Grape orchard was always well-irrigated and non stressed.

Linear regression analysis (A) was performed between the ETo estimates by the standard and comparison methods as follows:

$$ET_{Penman\text{-}Monteith} = A * ET_{method} \qquad \text{Eq. 35}$$

where A=regression coefficient. Regression through the origin was selected to evaluate the goodness of fit between the ET method estimates and the Penman-Monteith estimates because both values should theoretically approach the origin when the actual ET is zero.

Normalized error (NE) was calculated as: 100 * A

Results and Discussion

The study has revealed that some parameters in the M-SEBAL model are very sensitive. This can bee seen from the values of surface parameters derived from satellite image data. Figure 6 shows results of data processing for different land surface parameters and calculation of ET for the study area from NOAA-AVHRR (right) and LANDSAT-5 TM (left) satellite images.

By comparing figures 6,7 and 8 it is found that areas which have a low surface albedo and a low surface temperature have a high vegetation index and high evapotranspiration ; the other land areas which have low vegetation indices tend to have high surface albedo and temperature and low evapotranspiration. This is seen in figure 5a especially the part near the valley which represents the high vegetation density, while the part far from the valley area has the opposite situation.

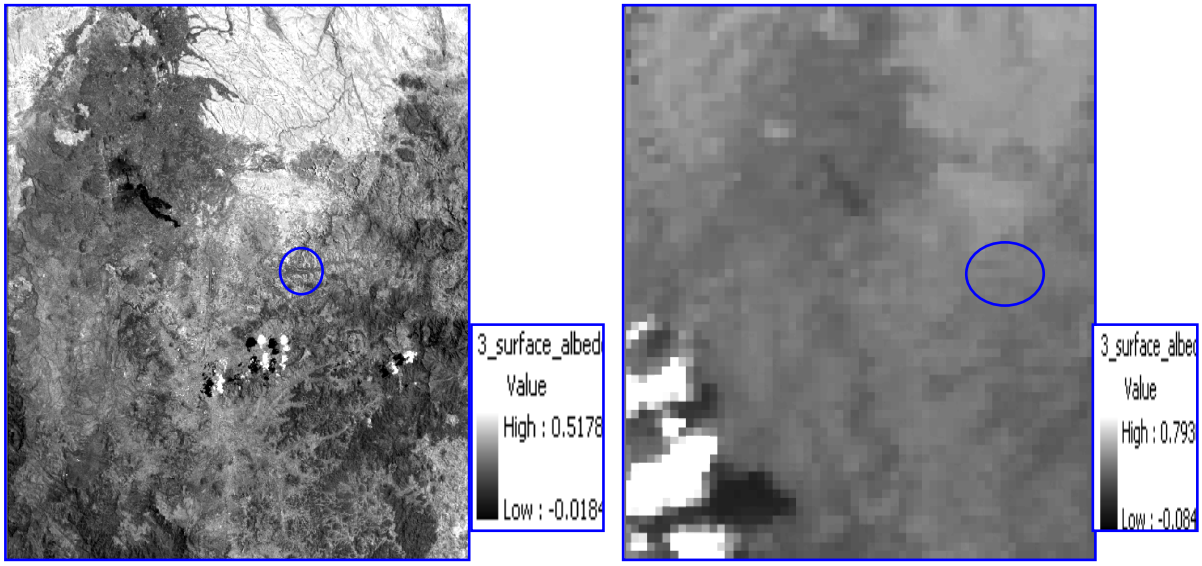

Figure 6 Estimated Surface Albedo derived from NOAA-AVHRR(right) and LANDSAT 5 TM (left) for Sana'a basin Yemen.

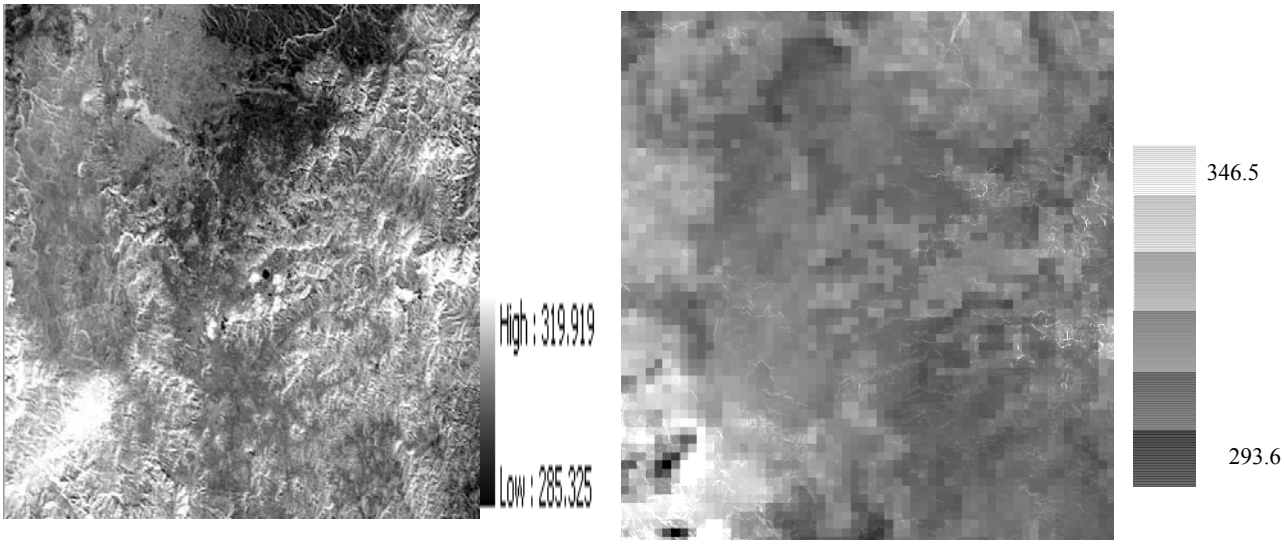

Figure 7 Estimated Surface Temperature (in K) derived from NOAA-AVHRR (right) and LANDSAT 5 TM (left) for Sana'a basin Yemen.

Figure 8 shows that daily ET is increased from bare soil to where Vegetation indices are high, the daily ET distribution by NOAA- AVHRR (0.0-17.8mm/day) and from LANDSAT 5 TM (0.0– 13.5 mm/day) .

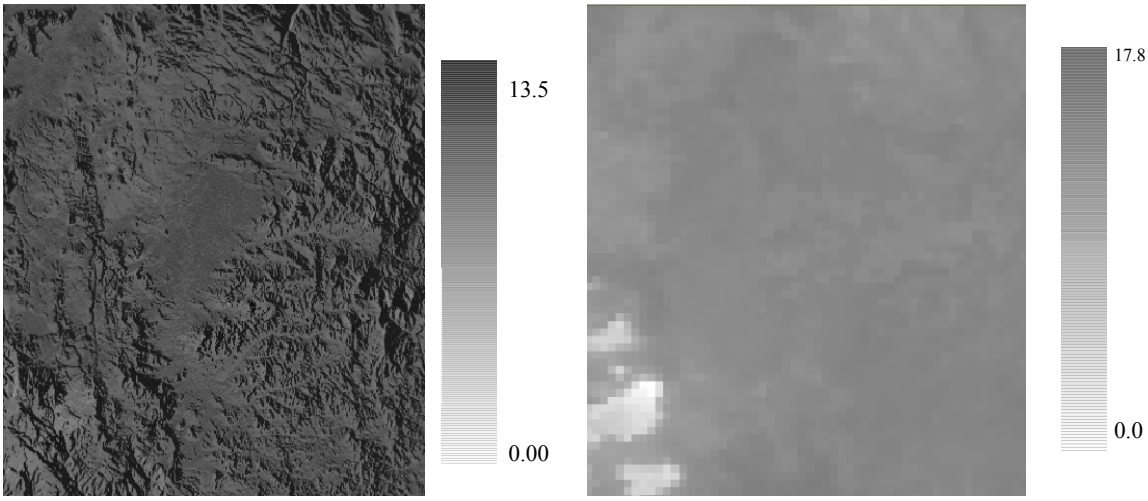

Figure 8 Estimated evapotranspiration averaged over 24 hours derived from NOAA-AVHRR(right) and LANDSAT 5 TM (left) for Sana'a basin Yemen.

The figures 9 and 10 show comparison values of surface parameters and land surface heat from both NOAA-AVHRR and Landsat TM satellite images over the study area (Sana'a, Basin), which comprises arid and semi arid conditions.

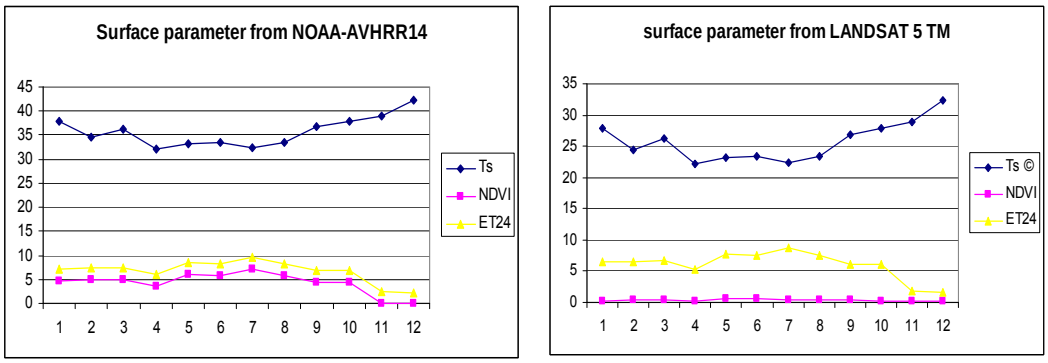

Figure 9. Estimated the surface parameter derived from NOAA-AVHRR (left) and LANDSAT- TM (right) on Sana'a Basin from TM, on 1st June 1998, T_s surface temperature, *NDVI* vegetation indices, ET_{24} evapotranspiration from satellite overpass time.

Figure 10 presents the results of the estimated surface heat fluxes over the study area from NOAA- AVHRR and from LANDSAT 5 TM (w/m^2). The latent heat flux (LE) is increased from bare soil to the vegetated area as ET.

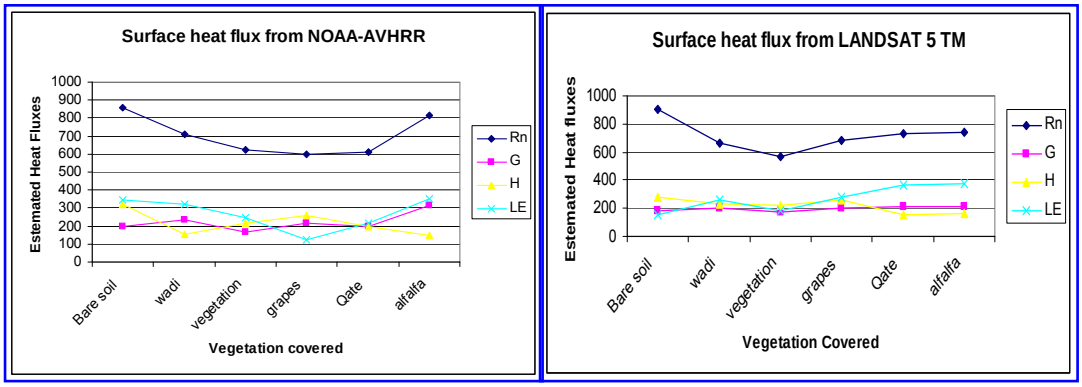

Figure 10. Estimated surface heat fluxes over arid and semi-arid region of Sana'a Basin from NOAA-AVHRR (left) and LANDSAT-5 TM (right). LE = latent heat flux, R_n = net radiation, G = soil heat flux, H = sensible heat flux.

Fusion Results

The result of the daily measured ET was compared with the M-SEBAL Landsat ET on four different dates during the growing season. Two out of 4 days show good agreement: the difference between measured and estimated daily ET is 0.1 mm on Dece 24th and 0.5 mm on June 1st (see Fig. 11). On the Landsat image of June 1st some haze was present above a large part of the Sana'a basin irrigation district including the measurement site. Due to haze an area appears colder on the satellite image than it actually is, causing higher M-SEBAL ET values. On March 26, measured value is 1.0 mm higher than the M-SEBAL ET. This difference for the Landsat day appears consistent with the NOAA-AVHRR results: March 31 NOAA-AVHRR and both estimates are higher than the landsat TM and measured values.

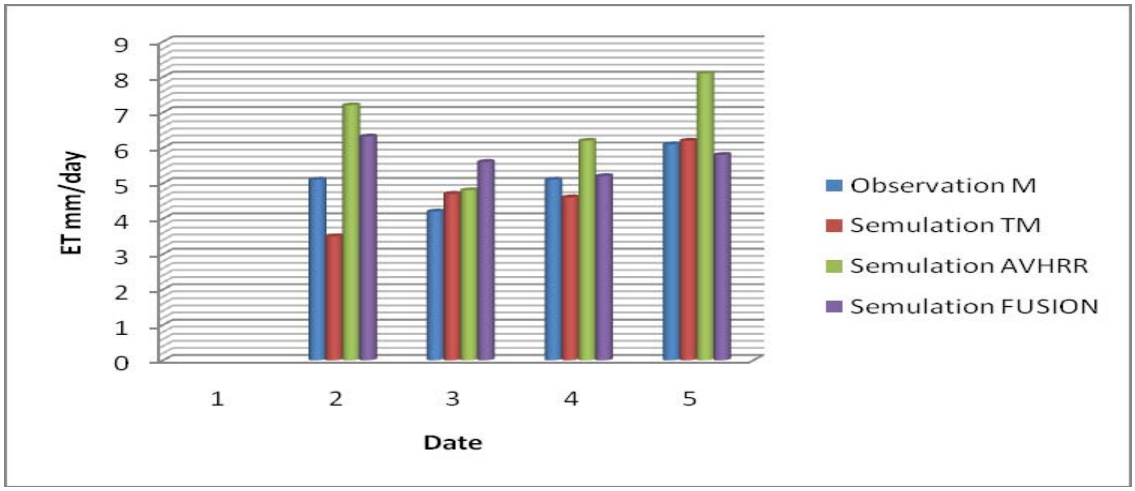

Figure11. Measured daily ET plotted against SEBAL daily ET of four TM & AVHRR actuation dates and daily ET of the integrated LANDSAT-NOAA ET computed according to eq.2

Working in the field of multi-sensor image fusion, the evaluation of the achieved results becomes relatively complex because of the different sources of data that are involved (Pohl and Van Gendren, 1998). It is even more difficult when multi-date composite data are used for data fusion. One of the possibilities

is to validate findings from fused data by comparing with actual data sets or ground truth (Pohl and Van Gendren, 1998). In this study, for the purpose of validation, the classified image of NOAA-AVHRR-LANDSAT TM fused image was compared with classified image of Landsat TM data acquired at the same time as NOAA-AVHRR. Figures 8 ET result from AVHRR (right) TM (left) and fig. 12 fusion ET. The result image demonstrate classification result of NOAA-AVHRR composite image, NOAA-AVHRR –TM fused image and Landsat TM image acquired during early June 1996. The comparison of images covering of the Sana'a basin Yemen clearly shows the spatial improvement in the classification accuracy in the fused image.

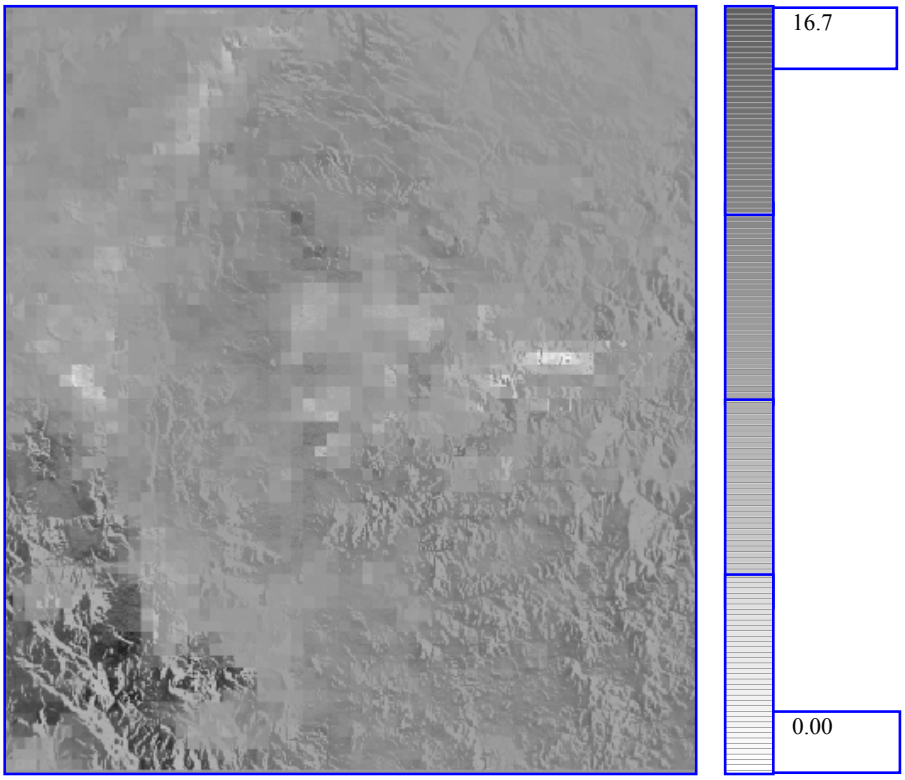

Figure 12. Evapotranspiration SEBAL fused image June 1998)

For numerical comparison, the statistics of ET derived from the NOAA-AVHRR composite image, fused image and Landsat image are given in table2. This shows a slight improvement in the classification result of fused data. Further detailed comparison will be made using better ground truth data, which is being collected in the Landsat TM images in Sana'a basin.

Table 2. Observation PM and Simulation TM, AVHRR and Fusion ET in Sana'a basin area

Observation PM	Semulation TM	Semulation AVHRR	Semulation FUSION
5.1	3.5	7.2	6.32
4.2	4.7	4.8	5.6
5.1	4.6	6.2	5.2
6.1	6.2	8.1	5.8

The model for grape fields is accurate (Table 2, Figure 11).

The accuracy assessment and error analysis for daily ET

The accuracy of M-SEBAL strongly depends on the quality of the thermal information which is used to retrieve the radiometric surface temperature of the pixel. Table 3. shows a summary of the results obtained in the model validation. ET values from M-SEBAL were obtained averaging results from four 30 m x 30 m pixels approximately centered at the soil water balance (lysimeter) site in the Experimental Farming – Faculty of Agriculture (EFFA), Sana'a University. Table 3 includes the values of ET_{24} (around the five days to the satellite overpass time) estimated from M-SEBAL, and corresponding ET_{24} measured at the lysimeter site. In addition, the corresponding values of reference ET are included for comparative purposes.

Table 3. Summary of ET Comparison for 1998 (sorghum), 1995 (alfalfa), and 1995 (peas) EFFA by ET calculated by M-SEBAL model using Landsat TM images

Date	ET-Lysimeter	ET-TM	AE	RE	A	NE
1st JUNE1998	6.91	5.281	1.629	0.235	0.764	76
12th december1995	4.05	3.414	0.636	0.157	0.842	84
20th MAY1995	7.98	5.91	2.07	0.259	0.740	74

ET-lysimeter = Measured ET values were provided by EFFA archive, 2006
ET-TM= ET calculated by M-SEBAL model using Landsat TM images
AE= The Absolute Error.
RE= The Relative Error.
A= Difference $ET_{(PM)}$ / $ET_{(LYSI)}$ (linear regression coefficient).
NE= Normalized error was calculated as 100*Difference
Negative value in ET difference indicates that ET-TM was lower than the lysimeter ET.

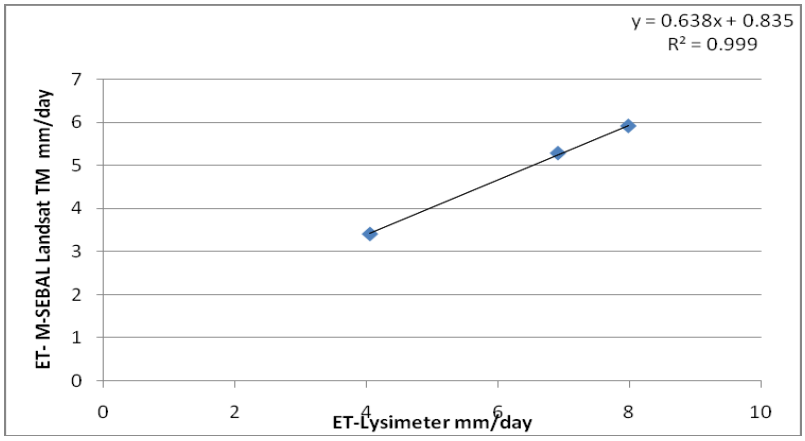

Figure 13 Remote sensing estimated ET versus with the lysimeter water balance ET.

The ET estimated by the remote sensing method versus ET estimated by lysimeter water balance ET on the three days is shown in Figure 13. Their relationship can be shown as

$$ET_{TM} = 0.638\, ET_{lysimeter} - 0.835, \qquad r^2 = 0.999.$$

where ET_{TM} is the remote sensing method ET M-SEBAL model using Landsat TM images, and $ET_{lysimeter}$ is the lysimeter water balance method ET. The correlation coefficient indicate a strong relationship between the remote sensing ET and the lysimeter water balance ET.

As shown in Table 3, the Absolute error of the estimate of remote sensing , Landsat TM recorded ET and lysimeter water balance ET was 1.629 and 2.07 for EFFA station may20th 1995 and 1st June1998, respectively. The largest Normalized error (84%) was with the EFFA lysimeter on 12th december1995. The smallest Normalized error (74%) was with the EFFA lysimeter on may20th 1995.

Average monthly ratios of actual to potential ET in a long term lysimeter study from EFFA area in Sana'a basin could provide a more reliable monthly λET for the ET estimation in Sana'a basin, Yemen. This result supports the conclusion that M-SEBAL can accurately estimate ET for agricultural conditions. Table 4 includes the values of ET_{24} estimated from FAO Penman-Monteith equation, and corresponding ET_{24} measured at the lysimeter site. In addition, the corresponding values of reference ET are included for comparative purposes.

Table 4 Summary of ET Comparison for 1998 (sorghum), (peas) 1995, and (alfalfa) 1995 by ETc calculated by FAO Penman-Monteith equation in EFFA.

Date	ET-Lysimeter	ET-PM	AE	RE	A	NE
JUNE1998	6.91	5.8	1.11	0.160	0.839	84
december19995	4.05	6.723	2.673	0.397	0.602	60
MAY1995	7.98	5.3	2.68	0.335	0.664	66

$ET_{-lysimeter}$ = Measured ET values were provided by EFFA archive, 2006. ET_{-PM}= ET calculated by FAO Penman-Monteith equation. AE= The Absolute Error., RE= The Relative Error. A= Difference $ET_{(PM)}$ / $ET_{(LYSI)}$ (linear regression coefficient). NE= Normalized error was calculated as 100*Difference

The ET estimated by the lysimeter water balance ET method versus ET estimated by traditional (FAO Penman-Monteith) method at EFFA weather stations on the three days is shown in Table 4 . The correlation coefficient indicates a strong relationship between the lysimeter water balance ET and the FAO Penman-Monteith method ET.

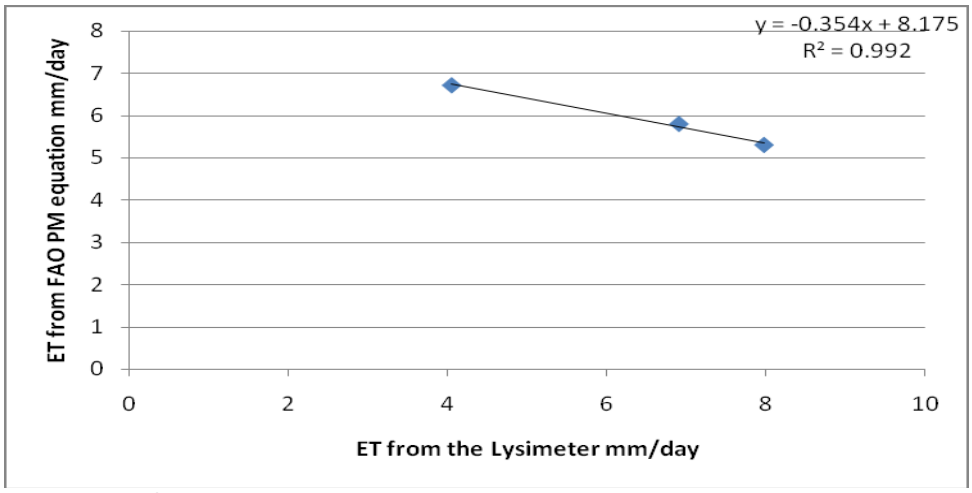

Figure 14 FAO Penman-Monteith estimated ET versus with the lysimeter water balance ET.

Table 5 Comparison of surface parameter using NOAA-AVHRR and Landsat-TM Images EFFA

DATE	DATA	TM	AVHRR	AE	RE	A	NE
1st June 1998	NDVI	0.54	0.27	0.27	0.5	0.5	50
	Ts	307.9	314.7	6.8	0.022	0.978	98
	ET	6.28	4.833	1.447	0.230	1.299	130
12th December 1995	NDVI	0.415	0.324	0.091	0.219	1.281	128
	Ts	307.2	315.2	8	0.026	0.9759	97
	ET	3.8	3.77	0.03	0.008	1.008	101
20th May 1995	NDVI	0.59	0.324	0.266	0.451	1.821	182
	Ts	309	314.5	5.5	0.018	0.982	98
	ET	4.85	4.22	0.63	0.129	1.149	115

AE= the Absolute Error. RE= the Relative Error. A= Difference $ET_{(PM)}$ / $ET_{(LYSI)}$ (linear regression coefficient). NE= Normalized error was calculated as 100*Difference

As shown in Table 5, the Absolute error of the estimate of remote sensing , Landsat TM recorded ET and NOAA-AVHRR ET was 0.03 and 1.447 for EFFA station December 13th 1995 and 1st June 1998, respectively. The largest Normalized error (130%) was with the EFFA lysimeter on June 1st 1998. On that date, the NOAA-AVHRR satellite image pixel at the EFFA lysimeter location was not identified as cloud-contaminated while the sorghum pixel was. However, the NDVI of the EFFA was significantly lower than the average NDVI

from other dates. The cause of the low NDVI value might be due to the existence of thin cloud which was not detected by the cloud screening algorithm. The low NDVI resulted in a low EF and consequently a low estimated ET.

Conclusion

This study has been able to that demonstrate the M-SEBAL is capable of calculating the surface parameters such as surface albedo, surface emissivity, vegetation index, surface temperature. They are significant important to estimate ET at regional scale. And the surface parameters can be accurately derived from satellite image data. In this case surface parameters have been derived from LANDSAT 5 TM and NOAA-AVHRR data; with the help of ground truth weather data values of derived surface parameters are validated to gauge the accuracy.

Due to improvement of the parameterization schemes for calculating the instantaneous and daily net solar radiation required in M-SEBAL, combined with remote sensing and metrological data and DEM, the detailed spatial distribution of ET from mountainous, trains was obtained. The variation in ET estimation of farming land in the valleys and bare lands with different fractional vegetation cover will lead to a change in processes and mechanisms of water-heat transfer, and M-SEBAL model performs well for high fractional vegetation cover area but poorly for moderate and low covers. The explicit spatial distribution of ET could be used for various purposes, which includes estimating soil moisture and predicting runoff, and other water-related research on watersheds.

Attempts were made for the first time in Yemen to find out statistical relations between NOAA-AVHRR and ground measured evaporation fraction of Landsat TM and evaporation fraction using the data from three different metrological station.

These relations would be helpful to extrapolate to larger areas. Moreover, the outputs of daily ET from M-SEBAL using the integrated LANDSAT 5 TM and NOAA-AVHRR data with DEM and ground observations were validated with daily ET from well-calibrated water balance simulation model.

The fusion of NOAA-AVHRR composite and Lansat TM is an effective method in image processing which improves spatial detail whilst maintaining the spectral signature very close to the original. Therefore one can clearly identify the ET at the period of NOAA-AVHRR data acquisition. Moreover, it improves classification accuracy. The technique is seen as the first stage of a process in which free, coarse resolution NOAA-AVHRR composites can be analyzed using a variety of multi-temporal techniques, ranging from characteristic signature extraction or through non-parametric approaches such as decision trees. This is the focus of continuing work to evaluate appropriate and affordable methods of regional ET. The technique is amenable to automation as the co-registration between NOAA-AVHRR composite data and the LANDSAT TM images are very good.

The methodology proposed in this study proved to be accurate in estimating seasonal ET at field level. The Penman Monteath PM observation measurements of ET correlated well with M-SEBAL estimated ET. The simulated is accurate compared to the measurement under both stressed and no stressed conditions. The future aim is to compare ET from different satellite estimation techniques and evaluate accuracy by comparing generated ET with continuous diurnal measurements throught the year using Bowen ratio towers at different agroclimatic zones in Yemen.

Acknowledgements

The authors gratefully acknowledges financial support for this research from the Islamic Development Bank (IDB), the satellite image data LANDSAT TM from the National Water Resources Authority (NWRA) government of Yemen, And the NOAA-AVHRR images and SRTM –DEM image from NASA website.

References

Allen, G.R., Pereira, L.S., Raes, D. and Martin, S., 1998, Crop evapotranspiration: guidelines for computing crop water requirements. *FAO Irrigation and Drainage Paper* 56, 300.

Almhab, Ayoub and Ibrahim Busu , 2008,Estimation of Evapotranspiration with Modified SEBAL model using landsat-TM and NOAA-AVHRR images in arid mountains area, EMS2008) EDAS(I EEE), Kuala Lumpur, Malaysia.

Almhab,A.& I. Busu, (2007a). Estimation of regional scale evapotranspiration for arid area using NOAA-AVHRR application in republic of Yemen, MAPASIA2007, Kula Lumpur , Malaysia.

Almhab, A. , I Busu, and N. ibrahim, (2007b). Estimation of regional evapotranspiration for Arid Areas Using LANDSAT Thematic Mapperarid Mapper for Grape Plantation, ISG & GPS/GNSS 2007, Johor ,Malaysia.

Almhab A., I. Busu, and A. Cracknell, (2007c). Comparison of regional evapotranspiration using NOAA-AVHRR and LANDSAT-TM images: a case study in arid area in the Sana'a basin, republic of Yemen, The 28th Asian Conference on Remote Sensing (ACRS) 2007P.N. 93, Kuala Lumpur, Malaysia.

Bastiaanssen, W. G. M., E. J. M. Noordman, H. Pelgrum, G. Davids, B. P. Thoreson, and R. G. Allen, 2005: SEBAL model with remotely sensed data to improve water-resources management under actual field conditions. J. Irrig DrainageEengin, 131, 85-93

Bastiaanssen, W.G.M., 2000, SEBAL-based sensible and latent heat fluxes in the irrigated Gediz Basin, Turkey. Journal of Hydrology 229(1/2), 87–100.

Bastiaanssen, W.G.M., Menenti, M., Feddes, R.A. and Holtslag, A.A.M., 1998, A remote sensing surface energy balance algorithm for land (SEBAL) 1,2. Formulation. Journal of Hydrology 212/213, 198–212.

Bastiaanssen, W.G.M., 1995, Regionalization of Surface Flux Densities and Moisture Indicators in Composite Terrain. A Remote Sensing Approach under Clear Skies in Mediterranean Climates (Wageningen: Agricultural Research Department).

Brutsert, W., 1979, Heat and mass transfer to and from surface with complete vegetation or similar permeable roughness. Boundary Layer Meteorology 16, 365–388.

Burggeman H.X. 1997.Agro Climat Resources of Yemen , part 1 , Agro Climat Inventory , FAO project, gcp,YEM/021/NET,Field doc.11, Ministry of Agriculture and Irrigation, Agriculture Research and Extension Authority (AREA), Dhamar, Yemen.

Chemin,Y. Z,. kiysosh A. and Amor V. (2004), “Genetic algorithm for assimilating remotely sensed Evapotranspiration using SWAP model implementation issues,Proceeding of the FOSS/GRASS User conference – Bangkok, Thailand, 12-14 Sep.2004.

Chemin,Y. Z,. (2002), “Problems in the Fusion of Commercial High-Resolution Satellite as well as Landsat 7 Images and Initial Solution,” Symposium on Geospatial Theory, Processing and Applications, Ottawa.

Chemin, Y., and Ahmad, M.D., 2000. Evaporation calculation from an Energy Balance model (SEBAL) A manual. IIMIPakistan Blue Report N° 102, Lahore, Pakistan, 27p.

Campbell, G.S.and Norman, J.M., 1998, An Introduction to environment biophysics (New York: Springer).

Doorenbos, J. and Pruitt, W.O., 1977, Crop water requirements. FAO Irrigation and Drainage Paper 24, 156.

DuffieJ.A and W.A.Beckman. 1991. Solar engineering of thermal process. 2nd Ed. John Wiley and sons, NY

ERDAS, 1995. ERDAS Field Guide, 3rd ed. Atlanta, Georgia, pp.628

Stull, R. B., 2001: An introduction to boundary layer meteorology. Kluwer Academic.

Tasumi, M., Bastiaanssen, W.G.M. and Allen, R.G., 2000, Application of the SEBAL methodology for estimating consumptive use of water and stream flow depletion in the Bear River Basin of Idaho through remote sensing. EOSDIS Project Final Report, Appendix C.

Van de Griend, A.A. and Owe, M., 1993, On the relationship between thermal emissivity and the normalized divergence vegetation index for natural surfaces. International Journal of Remote Sensing 14, 1119–1131.

Wing J, Sammis T.W, Meier C.A, Simmons L.J, Miller D.R, Samani Z, 2006, A Modified SEBAL model for spatially estimating pecan consumptive water use for las cruces, New Mexico, Agronomy and Horticaulture Departement, New Mexico State Univ. Las Cruses, New Mexico, USA.

Phol, C., and J.L. Van Genderen,(1998), " Multisensor Image Fusion in Remote Sensing: Concepts, Methods and Applications," International Journal of Remote Sensing, vol 19, no. 5, p.p 823-854, 1998.